Modeling Tritium Interactions with Metals

Introduction

Quantitatively modeling the interaction of tritium with metals is a vital step toward understanding the mechanisms of tritium migration through the metal. In turn, understanding these fundamental mechanisms is necessary to interpret experimental results and to make accurate predictions regarding tritium migration in metals during exposures to tritium gas and subsequent storage periods and/or cleaning procedures. While the literature contains several attempts at creating a quantitative model,[1–4] each attempt lacks one fundamental aspect: tritium migration across the surface–metal lattice interface. Many reports in the literature show that tritium adsorbs onto the surface as tritiated water,[1,5,6] while tritium absorbs into the metal lattice as atomic tritium.[5] This difference in retention media results in the measured large differences in tritium concentrations in the surface and in the bulk metal.[7] Including this physical condition into a quantitative model is necessary to accurately model the complete tritium–metal system.

In this article, we present a quantitative tritium migration model (QTRIMM) for modeling tritium migration in various metal substrates. This model includes the surface film of adsorbed water and relates the concentrations of tritium within the thin film of adsorbed water to the tritium concentrations within the substrate metal. Additionally, the tritium concentrations throughout the metal sample are output from the model calculation. Currently, this information is obtained experimentally only through acid etching or other destructive techniques. The model developed in this work provides two major advantages. First, inclusion of the thin film of adsorbed water in the model provides the first step toward a global model, capable of describing all experimental conditions. Second, because the tritium concentration profiles throughout the sample are calculated, the model has the potential to predict the location of tritium within a metal using only the loading and storage conditions. This avoids the necessity of destructive techniques to determine the tritium concentration profiles. Further, the model can be used to calculate the increase in gas-phase protium concentrations in a mixture of deuterium and tritium.

In this article the physical picture of a metal's surface is presented first, along with the primary assumptions and the relevant equations. Following this, a detailed derivation of the model is included. This derivation is divided into two major parts: bulk migration and surface conditions. To model tritium migration in the bulk metal lattice, Fick's second law of diffusion is solved numerically. This solution includes a condition for tritium diffusion through composite media. Next, the surface boundary conditions used to model tritium migration during an exposure to tritium gas and during a subsequent storage period are presented. Finally, a few predictions are made by using QTRIMM.

Surface–Metal Interface Condition

Tritium interacts with metal substrates by first adsorbing onto the metal surface and then permeating through the metal lattice. Under most conditions, tritium does not adsorb directly onto the metal's surface. Instead, the tritons adsorb in the form of tritiated light water (HTO).[1,5,6] After adsorption onto the surface, tritium can migrate from the water layers into the bulk metal lattice. The tritons occupy interstitial locations and defect sites within the metal's crystal lattice and diffuse through the lattice by migrating between the various sites. This process is illustrated in Fig. 150.39. Here, the approximate thickness of both the water layers and the metal oxide layers are shown for reference. The remainder of this section will address the tritium migration mechanisms treated in QTRIMM and will discuss the major assumptions of the model.

The first step in the tritium permeation process is adsorption onto the metal surface. This process presumably occurs through isotope exchange between tritiated species in the gas phase and water molecules adsorbed on the metal surface.[6] This exchange process is expected to occur rapidly, relative to tritium migration into the underlying metal lattice. Assumption of rapid equilibrium across the surface–gas interface is justified by comparing the flux of gaseous tritium to the surface and the diffusive flux of tritium into the metal lattice.[8] Additionally, the average residence time of adsorbed species is of the order of femtoseconds at 25°C.

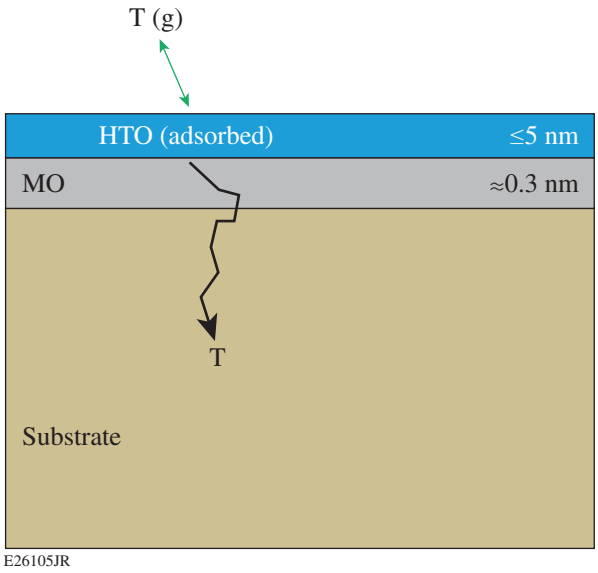

Figure 150.39
Illustration of tritium adsorption and migration into a metal sample. The adsorbed water layers and metal oxide (MO) layers are depicted on the surface of a metal substrate.

Rapid equilibrium across the surface–gas interface makes it possible to determine the surface concentration of tritium. At equilibrium, the surface concentration of tritium is related to the concentration of tritium within the gas phase

$$\chi_{\text{surf}}^{\text{eq}} = f * \chi_{\text{gas}}^{\text{eq}}. \tag{1}$$

In this formula, the mole fraction of tritium on the surface $\left(\chi_{\text{surf}}^{\text{eq}}\right)$ is related to the mole fraction of tritium in the gas phase $\left(\chi_{\text{gas}}^{\text{eq}}\right)$ by a constant factor (f). This factor accounts for various isotope exchange probabilities. In the limiting case of equal exchange probabilities, the scaling factor is unity. In reality, it is likely that the formation of double-isotope species, such as T_2O, is not as probable as the formation of mixed isotope species of water, such as HTO or DTO (tritiated heavy water). This more-realistic scenario of nonequal reaction probabilities would reduce the scaling factor to a fractional value ranging between zero and unity. For simplicity, we take $f = 1$ in our calculations.

Using the above relation between the mole fractions in the two phases makes it possible to determine the absolute concentration of tritium in the adsorbed water layers. Assuming the density of these water layers does not change significantly with each successive layer, the concentration of tritium on the metal's surface is given by

$$c_{\text{surf}}^{\text{eq}} = \frac{\chi_{\text{gas}}^{\text{eq}} * f * \rho_{H_2O}}{\delta_{\text{ML}}} * \frac{2\ \text{mol H}}{\text{mol H}_2\text{O}}. \tag{2}$$

Here, the concentration of tritium $\left(c_{\text{surf}}^{\text{eq}}\right)$ is determined by the mole fraction of tritium in the gas phase $\left(\chi_{\text{gas}}^{\text{eq}}\right)$, the isotope exchange scaling factor (f), the surface density of water $\left(\rho_{H_2O}\right)$, and the thickness of a monolayer of water (δ_{ML}). An additional factor of 2 is included to relate the number of moles of hydrogen to the moles of water on the surface. In the limit of $f = 1$, $c_{\text{surf}}^{\text{eq}}$ is taken to be equal to a saturated surface solubility S_{surf}. Under the assumptions of rapid equilibrium and a static gas phase, the equilibrium surface concentration in Eq. (2) remains constant throughout an exposure to tritium gas. In a situation where the fraction of tritium in the gas phase changes, the surface concentration will rapidly adjust to the new conditions.

After adsorption onto the surface, tritium can then permeate through the metal lattice by diffusing from site to site within the lattice. Permeation through the lattice begins with the triton crossing the surface–metal lattice interface. Migration across this interface is also assumed to be much faster than the rate of tritium diffusion in the underlying metal substrate. As such, the chemical potentials of tritium dissolved on either side of the interface are equal at the interface:

$$\mu_{\text{surf}}\left(x_{\text{I}}\right) = \mu_{\text{metal}}\left(x_{\text{I}}\right), \tag{3}$$

where μ_{surf} and μ_{metal} are the chemical potentials in the adsorbed water layers and the metal lattice, respectively, and x_{I} represents the position of the interface. This equality leads to a relation between the concentrations of tritium within each region:

$$\frac{c_{\text{surf}}^{\text{eq}}\left(x_{\text{I}}\right)}{c_{\text{metal}}^{\text{eq}}\left(x_{\text{I}}\right)} = \exp\left(-\frac{\mu_{\text{surf}}^{*} - \mu_{\text{metal}}^{*}}{RT}\right). \tag{4}$$

This equation states that the ratio between the equilibrium concentrations in each region (c^{eq}) depends on the standard chemical potentials in each region (μ^{*}), the gas constant (R), and the temperature (T). In a complete description of solute migration across an interface, the standard chemical potentials can vary from point to point as a function of depth. Varying standard potentials may result in gradual changes in the potential, culminating with equal standard potentials at the interface. Equal standard potentials result in equal concentrations at the

interface and therefore in a continuous solute concentration profile across the interface region. Including spatially variable standard chemical potentials may not be necessary since some physical situations can be modeled well with the simplified approach of constant chemical potentials.[9] Physical situations like this may be the result of well-defined boundaries between phases, similar to the interface between two solids. In these situations, the standard potential changes over a small distance are small and the equilibrium tritium concentrations at the interface are related by a constant factor.

The constant factor relating the tritium concentrations at the interface can be obtained by using Sievert's law, where the ratio of the tritium concentrations given by Eq. (4) is equal to the ratio of the solubilities of tritium in each region (S_i), assuming the partial pressure of tritium at the interface is a constant:

$$\frac{c^{\,\mathrm{eq}}_{\mathrm{surf}}}{c^{\,\mathrm{eq}}_{\mathrm{metal}}} = \frac{S_{\mathrm{surf}}}{S_{\mathrm{metal}}}. \tag{5}$$

This equation makes it possible to determine the tritium concentration in the metal lattice, given a tritium concentration on the surface. In order for the equality shown in Eq. (5) to hold, the metal lattice concentration must be multiplied by the isotope exchange scaling factor [Eq. (1)]:

$$\frac{c^{\,\mathrm{eq}}_{\mathrm{surf}}(f)}{f * c^{\,\mathrm{eq}}_{\mathrm{metal}}} = \frac{S_{\mathrm{surf}}}{S_{\mathrm{metal}}}. \tag{6}$$

For a constant temperature, the ratio of tritium solubilities in each region is a constant. Therefore, if the isotope exchange scaling factor is less than unity, the surface concentration will decrease, which means the concentration in the metal lattice must also decrease by the same factor.

This formalism for tritium migration across a boundary applies not only to transport across the adsorbed water–metal lattice interface but to any well-defined interface. One can extend Eqs. (3)–(6) to other composite media such as gold-plated metals or to metal substrates with artificially grown metal oxide layers, for example.

The final step toward describing tritium permeation is tritium diffusion through the metal lattice. For simplicity, we treat only lattice diffusion and ignore pathways such as grain boundaries and triple junctions and trap sites such as dislocations and vacancies. While these can be notable defects, the majority of the dissolved tritium is expected to migrate through the interstitial lattice sites in well-behaved metals with negligible contributions from defect sites.

Modeling Tritium Migration in the Bulk Metal Lattice

A model based on Fickian diffusion of tritium through the metal lattice has been developed. This model numerically solves for the tritium concentrations throughout a metal and includes a condition for solute diffusion through different, but interacting media, as outlined in the previous section. The numeric solution uses an intermediate time step and divides the solid into N cells. For simplicity, the model uses a one-dimensional solution. The quantity of solute in each cell can be determined by multiplying the cell thickness (Δx) with the surface area of the sample used in an experiment.

The concentration in each cell c is determined from a flux balance of tritium entering and leaving each cell. Because of this, the flux F is calculated at the intermediate positions, $i\pm1/2$ as shown in Fig. 150.40. The rate of change in the solute concentration in each cell is determined by relating Fick's First and Second Laws to yield

$$\frac{\partial c}{\partial t} = -\frac{\partial F}{\partial x}. \tag{7}$$

The finite-difference fluxes at the intermediate positions are

$$F_{i+1/2} = -D_{i+1/2}\left(\frac{c_{i+1}-c_i}{x_{i+1}-x_i}\right), \tag{8}$$

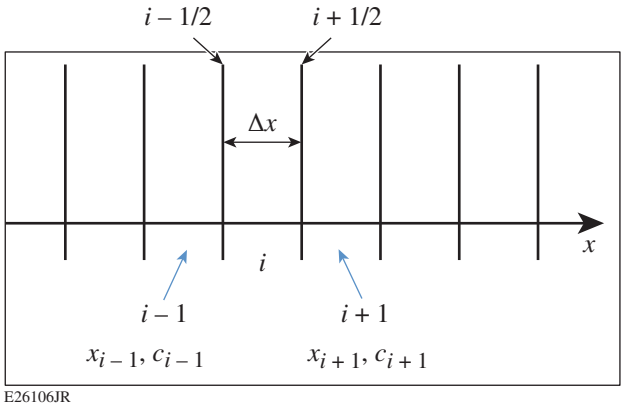

Figure 150.40
Division of solid into equally spaced cells.

$$F_{i-1/2} = -D_{i-1/2}\left(\frac{c_i - c_{i-1}}{x_i - x_{i-1}}\right), \quad (9)$$

where D is the diffusivity. Using Eqs. (7)–(10), the rate of change of the concentration in cell "i" is written as

$$\frac{c_i' - c_i}{\Delta t} = -\theta\frac{\left(F_{i+1/2}' - F_{i-1/2}'\right)}{\Delta x_i} - \frac{(1-\theta)\left(F_{i+1/2} - F_{i-1/2}\right)}{\Delta x_i}, \quad (10)$$

where the primes denote the next time step and θ is the degree of implicitness, which determines the degree of accuracy and stability; $\theta = 0.5$ provides the highest accuracy, while $\theta > 0.5$ enhances stability.

Equations (7)–(10) represent the basis for QTRIMM. Using these equations, a system of linear equations is obtained. Each equation in the set gives the concentration at the next time step for a particular location within the metal. Two additional equations are necessary to solve for the boundary conditions. These equations occur at indices of $i = 0$ and $i = N$ and will be discussed later. The total set of equations has one degree of freedom, allowing the system of equations to be solved exactly. Coupling Eq. (10) with a set of boundary conditions makes it possible to calculate the tritium concentrations in a homogeneous solid.

Tritium diffusion across an interface between two media requires that the flux equations [Eqs. (8) and (9)] be constrained. These fluxes must be modified to maintain a constant ratio of the tritium solubilities across the interface [Eq. (5)]. The other implicit condition is that the total quantity of tritium throughout the system must be conserved. Using these conditions, the equations for the modified boundary conditions can be derived.

To maintain mass balance throughout the system, the concentration at the interface must be given by the rate of solute entering and exiting the cell, i.e., we require flux balance. In the present diffusion model, the interface between two well-defined solvents is placed within one cell ($i = M$) in the discretized solid. The concentration at the interface position is then given by the average of the concentrations on the right $\left(c_M^R\right)$ and left $\left(c_M^L\right)$ sides of the cell because half of this cell is one solvent and half is the other:

$$c_M = \frac{\left(c_M^R + c_M^L\right)}{2}. \quad (11)$$

Combining Eqs. (5) and (11) yields

$$c_M^R = \left(\frac{2}{S_R + 1}\right)c_M = \varphi_R * c_M. \quad (12)$$

Similarly,

$$c_M^L = \left(\frac{2 * S_R}{S_R + 1}\right)c_M = \varphi_L * c_M. \quad (13)$$

The flux in and out of the interface cell must utilize c_M^L and c_M^R...

$$F_{M+1/2} = -D_{M+1/2} * \left(\frac{c_{M+1} - c_M^R}{x_{M+1} - x_M}\right)$$

$$= -D_{M+1/2} * \left(\frac{c_{M+1} - \varphi_R * c_M}{x_{M+1} - x_M}\right), \quad (14)$$

$$F_{M-1/2} = -D_{M-1/2} * \left(\frac{c_M^L - c_{M-1}}{x_M - x_{M-1}}\right)$$

$$= -D_{M-1/2} * \left(\frac{\varphi_L * c_M - c_{M-1}}{x_M - x_{M+1}}\right). \quad (15)$$

Equations (14) and (15) can be inserted into Eq. (10) to determine the concentrations around the interface ($i = M–1$, M, $M + 1$). These equations apply only around the interface position; the remaining equations are unchanged from the form derived for a homogeneous solid.

To solve for the concentration profiles in a metal sample, two equations for the boundary conditions are necessary. For the first boundary condition, we assume a symmetric solid. Under this assumption, the diffusion model must extend only to the center of the sample; the other side of the sample is a mirror image. To solve for the concentration at the centerline, we set the fluxes into or out of this cell to be equal but with opposite signs to reflect the opposite directions of flow. The boundary condition for the sample's surface depends on the experimental conditions. Two general cases are outlined in the following section: the first case treats a storage condition where tritium is allowed to redistribute throughout the solid as well as to desorb from the surface; the second case treats a

condition where a metal is exposed to gaseous tritium and is loaded with tritium.

Boundary Conditions at the Metal's Surface

We utilize slightly different surface boundary conditions, depending on whether the model calculates the concentration profiles during the loading phase or during a storage phase. During the loading phase, the surface concentration is assumed to be constant. During the storage phase, this concentration is allowed to vary because tritium is allowed to migrate into the metal lattice and to desorb from the surface at a constant rate. The derivations for these two conditions are shown below.

In all cases, multiple monolayers of adsorbed water develop on all metal surfaces that have been exposed to a humid atmosphere. These layers are distinct from the bulk metal and have a much higher solubility for tritium. To model tritium migrating from the bulk metal into the surface, the interface equations outlined in the previous section are used. Assuming that a rapid equilibrium develops across the surface–metal lattice interface, the concentrations on either side of the interface are related by the ratio of the solubilities for tritium in each region, as presented in Eq. (5).

The thickness of the metal substrate is much larger than the thickness of the adsorbed water layer as illustrated in Fig. 150.39. To account for this significant difference in thickness and to reduce the calculation time, two different cell sizes are used: one to calculate the concentrations in the bulk of the sample (Δx) and the other to calculate the surface concentration (δx). Given the small thickness of the water layer and the relatively slow rate of diffusion into the metal lattice, tritium concentrations likely equilibrate rapidly in the water layers relative to the bulk metal. Assuming this rapid equilibration and using the small water-layer thickness, the surface–metal interface is placed entirely in the first cell ($i = 0$) of the discretized solid as shown in Fig. 150.41. The thickness of the surface cell ($i = 0$) is determined by the surface concentration of adsorbed water (Q), the surface density of water $\left(\rho_{H_2O}\right)$, and the thickness of a monolayer of water (δ_{ML}):

$$\delta x = \frac{Q}{\rho_{H_2O}} * \delta_{ML} * 2. \tag{16}$$

The factor of 2 in this equation scales up the thickness of this cell to account for the fact that half of this cell is adsorbed water and half is the bulk metal lattice (Fig. 150.41).

For the loading phase, the surface concentration is assumed to remain constant in time. To incorporate this fixed concentration into the solution matrix, we assume a linear relation between the concentrations in the first three cells:

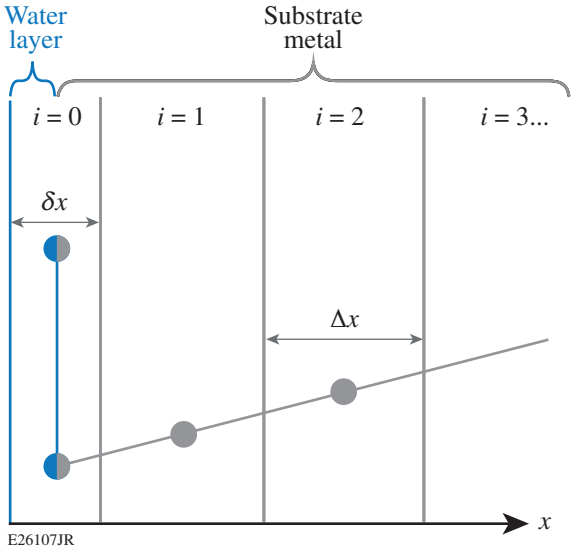

Figure 150.41
Illustration showing the position of the surface–metal lattice interface.

$$\frac{c_1' - c_0\varphi_R}{x_1 - x_0} = \frac{c_2' - c_0\varphi_R}{x_2 - x_0}. \tag{17}$$

This equation follows the same form as Eq. (10) and can be inserted directly into the system of equations defined by Eq. (10).

During the storage phase, the tritium concentrations in the surface cell ($i = 0$) are allowed to vary by including two conditions for tritium transport: diffusion into the metal and desorption from the surface. Following the same formalism shown above, we define the diffusive flux into the metal lattice as

$$F_{1/2} = -D * \left(\frac{c_1 - c_0 * \varphi_R}{x_1 - x_0}\right). \tag{18}$$

The desorbing flux away from the surface is defined by

$$F_{-1/2} = -\nu * c_0 * \varphi_L \left(\frac{\delta x}{2}\right), \tag{19}$$

where ν is the desorption rate constant. The return flux from the atmosphere to the surface is ignored in the equation because the airborne concentration is assumed to be negligible. The

thickness of the surface cell, δx, is divided in half since half of this cell represents the adsorbed water layers illustrated in Fig. 150.41. The desorption rate constant ν determines the rate at which tritium desorbs from the surface. Surette and McElroy measured this rate to be 0.91% per day for untreated stainless-steel surfaces.[10] This is equivalent to 10^{-7} tritons desorbing per second, which is the value used in the following calculations. Equations (18) and (19) can be inserted into Eq. (10) to yield the surface boundary condition in the diffusion model.

Model Predictions

Using the model outlined in the previous sections, we can predict the migration of tritium through a metal sample during an exposure to tritium gas, a subsequent storage period, and a decontamination procedure. The results of a series of simulations are presented in Figs. 150.42–150.44, which show the consequences of exposing stainless steel to tritium gas and then storing the metal for a period of time.

Table 150.III lists the hydrogen diffusivity in stainless steel, copper, and aluminum;[11] Table 150.IV lists the solubilities for these materials.[11] Figure 150.42 shows the calculated tritium concentration profiles that develop within a stainless steel sample, exposed to 612 Torr of hydrogen gas containing 60% tritium for 24 h. Initially, the surface concentration was fixed at the value shown, while the remaining concentrations in the metal were set to zero. The profiles are plotted in increments of 1 h. For clarity, only the concentrations within the metal lattice are shown; the high surface concentrations are off-scale. Using the final profile, we calculate that tritium penetrates a mean distance of ~10 μm into stainless steel. This compares favorably with the expected mean migration distance, which is found from the semi-infinite solution to the diffusion equation. The expected mean migration distance is

$$\langle x \rangle = \sqrt{4Dt} = 11.5\ \mu\text{m}, \tag{20}$$

where $\langle x \rangle$ is the mean migration distance, D in m^2/s is the diffusivity of tritium in stainless steel, and the exposure time t is 24 h.

Table 150.III: Hydrogen diffusivity in select materials.

	Stainless steel	Copper	Aluminum
Frequency factor (m^2/s)	7.2×10^{-7}	7.9×10^{-7}	1.46×10^{-6}
Activation energy (kJ/mol)	52.9	38.6	30.0
Diffusivity at 25°C (m^2/s)	4.1×10^{-16}	1.4×10^{-13}	5.0×10^{-12}

Table 150.IV: Hydrogen solubility in select materials.

	Stainless steel	Copper	Aluminum
Frequency factor ($mol/m^3 \cdot atm^{1/2}$)	342	1691	4416
Activation energy (kJ/mol)	13.0	39.3	28.5
Solubility at 25°C (mol/m^3)	1.8	0.22*	4.4×10^{-2}

*Scaled by 1000.

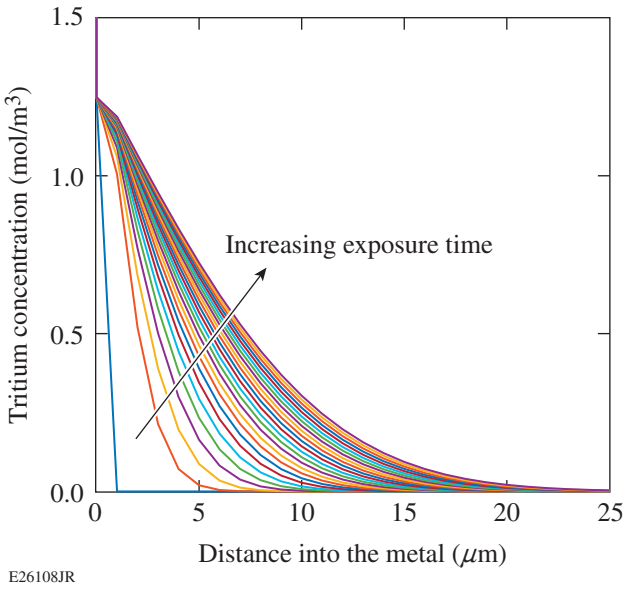

Figure 150.42
Evolution of tritium concentration profiles in stainless steel during an exposure to tritium. P = 612 Torr, $\chi_{tritium}$ = 0.6, t = 24 h, $Q = 10^{-5}$ mol/m^2.

In the second phase, the tritium profile evolution is tracked over a storage period of 50 days. During this time, tritium is allowed to redistribute throughout the metal, as well as to desorb from the surface. Tritium that has desorbed from the surface does not return to the sample in this example. The final concentration profile calculated for the loading procedure illustrated in Fig. 150.42 was used as the initial condition for the storage phase. The resulting concentration profiles in the metal lattice are shown in Fig. 150.43. Again, the high surface concentrations are not shown. Finally, the evolution of the concentration profiles are plotted in one-day increments. As expected the tritium concentrations in the near-surface region decrease while the tritium concentrations in the deeper regions increase with increasing storage time. This trend in the concentration profiles with increasing time produces profiles similar to those

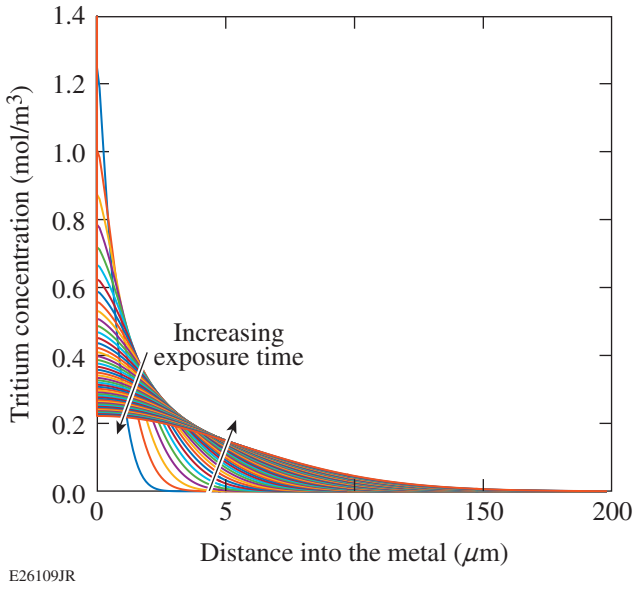

Figure 150.43
Tritium concentration profiles in stainless steel during storage following an exposure to tritium. P = 612 Torr, $\chi_{tritium}$ = 0.6, t = 24 h, $Q = 10^{-5}$ mol/m^2, $\nu = 1 \times 10^{-7}$/s.

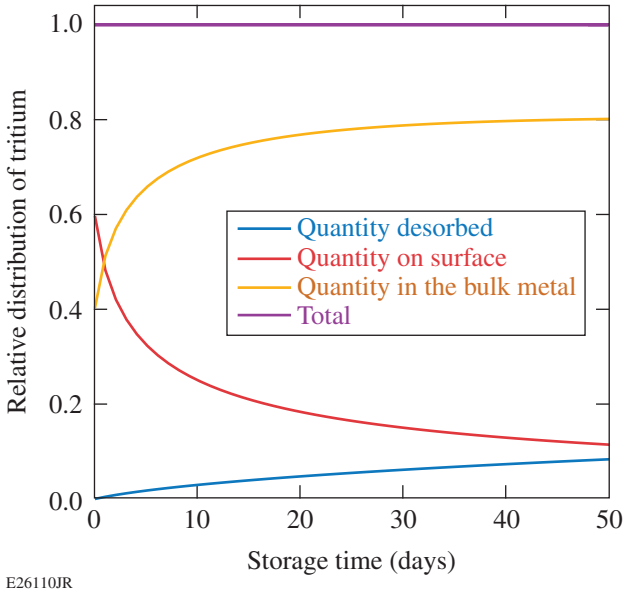

Figure 150.44
Dependence of relative distribution of tritium in stainless steel on storage time following an exposure to tritium. Included in this plot are the relative quantities of tritium that desorbed from the sample, as well as those remaining on the surface and in the bulk metal lattice. P = 612 Torr, $\chi_{tritium}$ = 0.6, t = 24 h, $Q = 10^{-5}$ mol/m^2, $\nu = 1 \times 10^{-7}$/s.

observed by Penzhorn *et al.*[7] These authors measured a local minimum in the concentration profile near the surface. They attributed this minimum to the chronic desorption of tritium from the surface, which is an effect predicted by the model.

Figure 150.44 shows the calculated relative distribution of tritium within the stainless-steel sample over the same storage period represented by the concentration profiles in Fig. 150.43. This figure shows the relative tritium inventories contained on the surface and in the bulk metal lattice along with the relative quantity that desorbed from the surface. For reference, the total mass of the system is also included. From these results, we can see that the surface contained ~60% of the total tritium inventory immediately after the 24-h exposure. This quantity rapidly decreases over the first ten days since tritium not only diffuses into the sample but also desorbs from the sample's surface. After ~30 days of storage, the relative distribution does not change significantly because the concentration gradients in the sample illustrated in Fig. 150.41 are less steep.

In the following example, a stainless-steel sample was exposed to various atmospheres of tritium gas for differing periods of time and then stored for either zero or one day prior to decontamination. The cleaning protocol was repeated over a ten-day period. In these two examples, the surface activity was reduced to zero during decontamination and the sample was stored for one day before repeating the cleaning procedure. During the storage periods, tritium could diffuse deeper into the sample as well as desorb from the surface. During loading, the surface concentration was fixed by the given exposure conditions and the tritium content in the sample bulk was set to zero. For reference, the 1000-DPM/dm^2 threshold is shown as a dashed line in each of the following two plots, where DPM is disintegrations per minute.

Figure 150.45 shows the activity on the metal surface immediately prior to the cleaning. The exposure and cleaning sequence indicates that tritium migrates back to the surface within each 24-h storage period. Further, regardless of the initial exposure conditions, the surface activity present after the first 24-h period indicates that the surface is above the 1000-DPM/dm^2 threshold. In all exposure cases considered, one additional decontamination was sufficient to bring the surface below the threshold. Additional decontaminations performed after the second day showed no significant depletion of the surface activity. A sufficient quantity of tritium is present within the metal lattice to replenish the surface with tritium to nearly the same level each following day.

Storing the sample for 24 h after an exposure significantly affected the residual surface activity after decontamination. Figure 150.46 shows the surface activity on the sample stored

for 24 h after exposure and before the first decontamination. In general, the results show that storing the samples for one day results in surfaces containing higher quantities of tritium after each decontamination cycle. Compared with the samples that were decontaminated immediately after exposure, most of the stored samples did not reach the target threshold, even after ten decay cycles. Storing the sample after exposure gave the tritium more time to diffuse into the bulk metal lattice. This higher reservoir of tritium in the metal in turn resupplied the surface with tritium, leading to the higher surface activities.

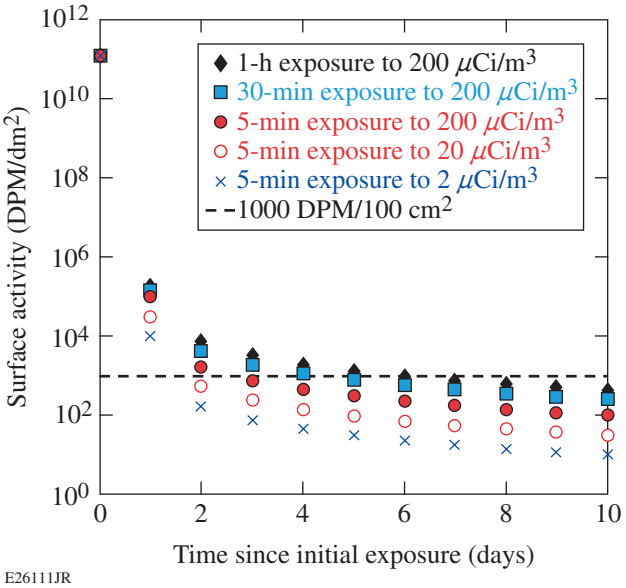

Figure 150.45
Dependence of surface activity on stainless steel on decontamination sequences without a storage period after exposure. The decontamination was repeated every 24 h for ten days. $Q = 10^{-5}$ mol/m^2, $\nu = 1 \times 10^{-7}$/s.

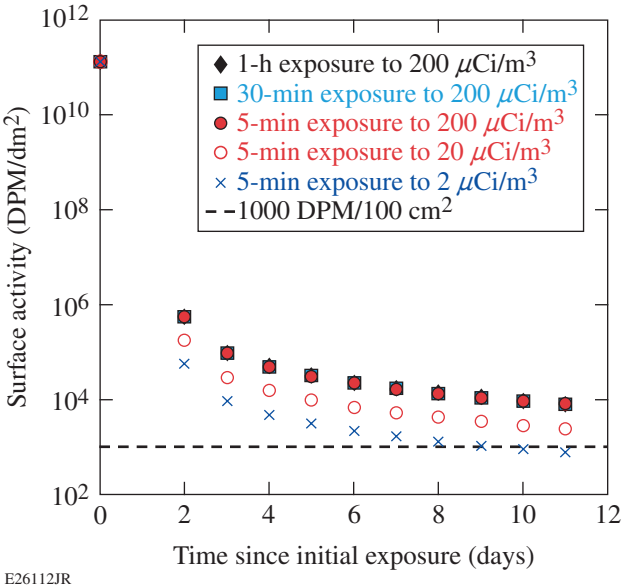

Figure 150.46
Dependence of surface activity of stainless steel on decontamination sequences following a one-day storage period after exposure. The decontamination was repeated every 24 h for ten days. $Q = 10^{-5}$ mol/m^2, $\nu = 1 \times 10^{-7}$/s.

The surface activity of aluminum after exposure to tritium and a series of subsequent decontaminations was also simulated. The operating conditions were identical to those used for stainless steel. As in the stainless-steel cases, two main scenarios were considered. In both scenarios (Fig. 150.47), the metal was exposed to a range of tritium gas concentrations for a variety of durations. In the first set of cases evaluated, decontamination proceeded immediately after exposure. In the second case, decontamination was initiated one day after the tritium exposure. In both cases, once the decontamination-dwell sequence was started, the surface was decontaminated after a 24-h hiatus over ten days.

The decontamination simulations indicate that more decontamination cycles are required for aluminum that was stored for one day prior to starting the decontamination sequence. The surface activity for the stored samples does not drop below the threshold until a minimum of seven decontamination cycles have been performed, compared to a minimum of two cycles for the case when the decontamination starts immediately after exposure. As in the stainless-steel case, the one-day storage period permitted tritium to permeate deeper into the bulk metal lattice. This leads to an increased reservoir of tritium in the lattice, which subsequently migrates to the surface after each successive cleaning.

For the same exposure conditions, stainless steel requires more decontamination cycles than aluminum when the exposed samples are stored for one day before starting the decontamination sequence. This difference is attributed to the fact that the diffusion of tritium into steel is 2×10^4 slower compared to aluminum. The higher diffusivity of tritium into aluminum expedites tritium migration to the surface after each cleaning. As a result, a greater fraction of the tritium inventory is removed from the bulk with each successive decontamination and the surface activity remaining after each 24-h period decreases faster on aluminum than on stainless steel.

The tritium exposure and decontamination protocols described above were repeated using 3-cm-thick aluminum instead of a 0.3-cm-thick sample (Fig. 150.48).

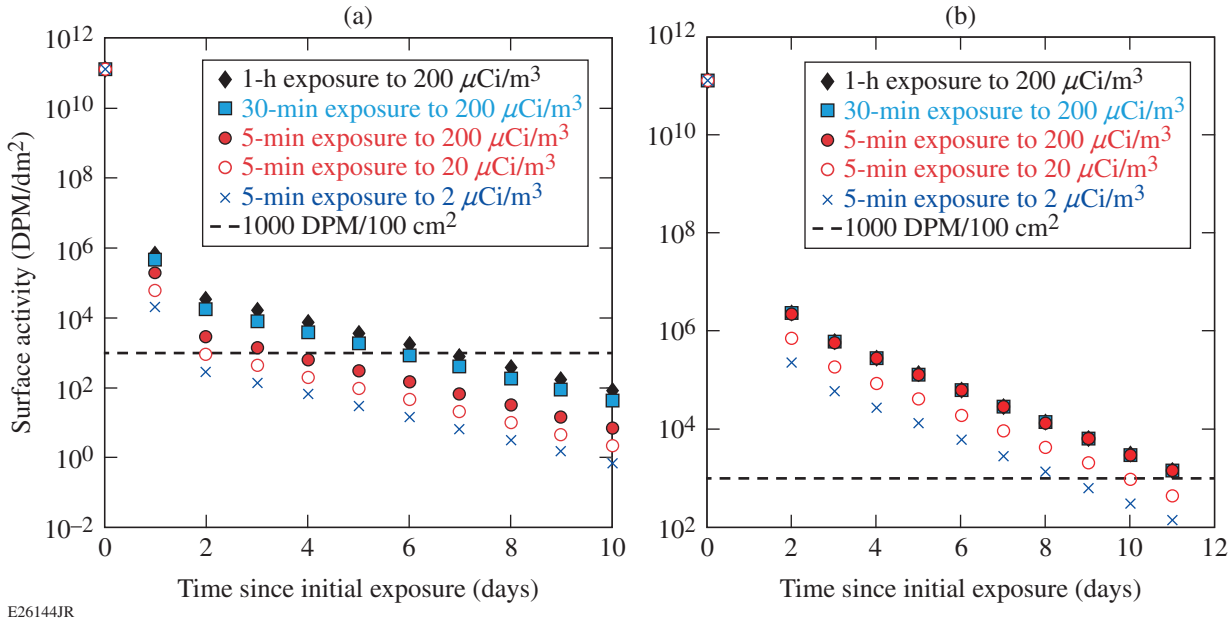

Figure 150.47
Decrease in the surface activity on 0.3-cm-thick aluminum calculated for a range of exposure conditions for two cases. (a) Decontamination was initiated immediately after exposure. (b) Decontamination was initiated one day after the exposure. The surfaces were decontaminated once every 24 h over a ten-day period in both cases. $Q = 10^{-5}$ mol/m^2, $\nu = 1 \times 10^{-7}$/s.

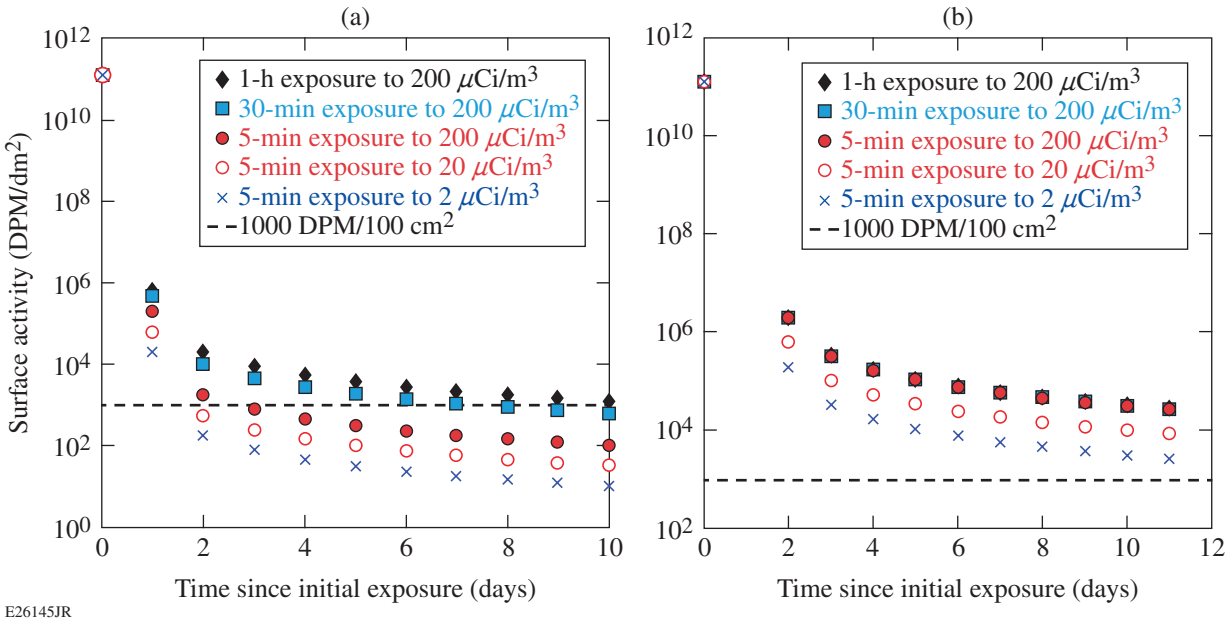

Figure 150.48
Decrease in the surface activity on 3-cm-thick aluminum calculated for a range of exposure conditions for two cases. (a) Decontamination was initiated immediately after exposure. (b) Decontamination was initiated one day after the exposure. The surfaces were decontaminated once every 24 h over a ten-day period in both cases. $Q = 10^{-5}$ mol/m^2, $\nu = 1 \times 10^{-7}$/s.

The calculations show that increasing the thickness of the aluminum results in higher surface activities throughout the decontamination process. For the immediate decontamination scenario, the surface activity remains above the target threshold for the higher tritium concentrations and longer exposure condition and drops below the threshold for the shorter periods and/or lower concentrations. In the delayed decontamination scenario, the residual surface activity does not drop below the threshold for any of the exposure cases considered. Additionally, the decay in the residual surface activity in both scenarios does not follow the trend observed for the 0.3-cm case illustrated in Fig. 150.47. In the 0.3-cm case, the residual surface activity decreased linearly after the second surface cleaning. In the 3-cm case, the residual surface activity decreases at a slower, nonlinear rate. The increased metal volume provides a larger reservoir for tritium in the 3-cm case for identical exposure conditions. Increasing the thickness of the aluminum allows tritium to migrate deeper into the bulk during the dwell periods between surface decontaminations because of the higher diffusivity of tritium in aluminum.

In the following example, a stainless-steel sample was exposed to a tritium atmosphere containing 5 μCi/m^3 until a steady state was reached. Afterward, the sample was subjected to the same decontamination cycles described above. The surface was decontaminated once a day for ten days where each decontamination was assumed to completely remove all surface-bound tritium. During the storage period between the surface cleanings, tritium repopulated the surface and could desorb from the surface. The results are shown in Figs. 150.49 and 150.50. Figure 150.49 shows the tritium concentration profiles in the bulk metal after each decontamination, while Fig. 150.50 shows the surface activity remaining prior to the next decontamination cycle.

Figure 150.49 shows that each successive decontamination further depletes the tritium content in the near-surface region. This depletion is in response to the removal of the surface activity and, consequently, the abrupt change in the tritium inventory at the interface on the metal side. The concentration gradient drives tritium to migrate out of the metal lattice and back into the surface layer. Storing the sample for one day between successive decontamination cycles provides the necessary time for tritium to migrate into the surface water layer. Increasing the storage time would increase the quantity of tritium migrating to the surface since tritium diffusion through the metal lattice limits the flux to the surface.

In addition to depleting the near-surface tritium with each decontamination, the simulation shows that the surface contamination cannot reach the 1000-DPM/dm^2 threshold within ten decontamination cycles. Figure 150.50 shows the evolution

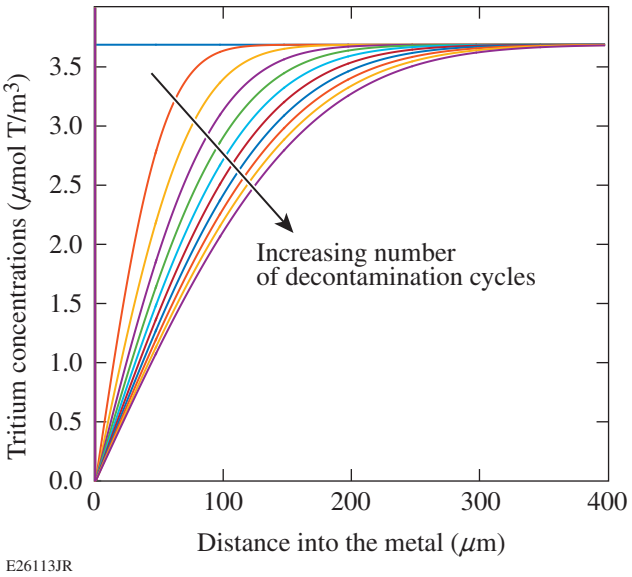

Figure 150.49
Evolution of tritium concentration profiles that develop in the bulk metal of stainless steel following sequential decontaminations after exposure to 5 μCi/m^3 of tritium in an inert environment until steady-state concentration profiles were reached in the metal. The profiles are plotted in one-day increments for sequential decontaminations. The initial profile is shown for reference.

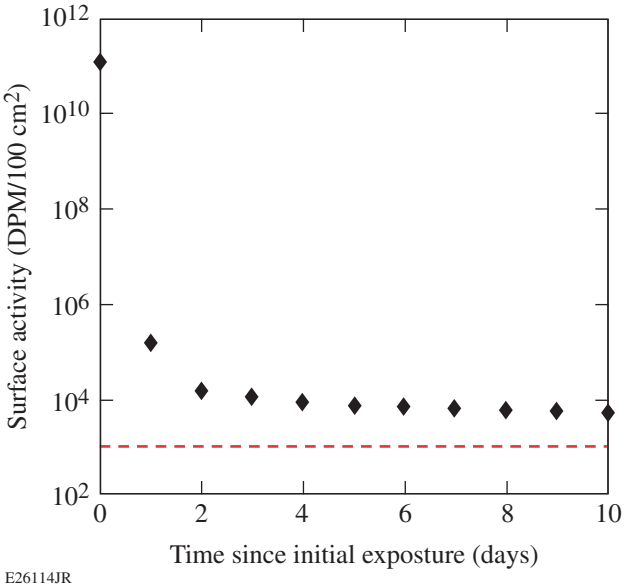

Figure 150.50
Dependence of the surface activity on decontaminations repeated once a day over ten days for stainless steel exposed to a tritium atmosphere of 5 μCi/m^3 for a prolonged period. The sample was stored for 24 h between decontaminations. $Q = 10^{-5}$ mol/m^2, $P_{\text{tritium}} = \mu\text{Ci/m}^3 = 3.2 \times 10^{-9}$ Torr, $\chi_{\text{tritium}} = 1$, $\nu = 1 \times 10^{-7}$/s.

of surface activities with sequential decontaminations. While the decontamination cycles reduce the residual surface activity to lower values, progress to puncture the 1000-DPM/dm^2 threshold is slow. The difficulty in reducing surface contamination is because of the vast reservoir of tritium present within the metal lattice.

QTRIMM can also be used to calculate the temporal evolution of tritium pulses applied to various metals. In the example under consideration, one side of a metal wall is exposed to a deuterium–tritium (DT) gas mixture at room temperature. Following the exposure, the DT gas is evacuated and the wall remains under vacuum for a specified period of time. This cycle of exposure followed by vacuum outgassing is repeated several times. The tritium concentration profiles and tritium distributions are calculated for each cycle. In these calculations, the downstream boundary condition is modified to include a high-solubility surface from which tritium can desorb. This condition is identical to that used for tritium desorption from a surface in Eq. (19) except that the flux is positive since the flow is in the opposite direction. The permeation calculations compare the performance of three metals: aluminum, copper, and stainless steel using the literature survey averages of the solubilities and diffusivities for the three metals listed in Tables 150.III and 150.IV. The solubility of tritium in copper was increased by a factor of 1000 relative to the literature survey average to account for the observed increase in hydrogen solubility in copper at low temperatures. The parameters listed in Table 150.V are used for this example for the three metals. We cannot assume that the quantity of water absorbed on the metal surfaces is the same for the three metals because these quantities are metal dependent.[6] Additionally, the desorption rates from the upstream and downstream surfaces may be different because of the different environments;[12] however, these parameters are not expected to differ significantly from metal to metal.

Table 150.V: Parameters used to calculate tritium permeation through the selected metals.

Mole fraction of tritium in the gas	0.7
DT pressure	50 Torr
Temperature	298 K
Quantity of adsorbed water on upstream (DT gas/vacuum) wall	10^{-5} mol H_2O/m^2
Quantity of adsorbed water on downstream (lab air) wall	5×10^{-5} mol H_2O/m^2
Desorption rate constant (both surfaces)	10^{-7}/s
Exposure time	100 h
"Storage" time	50 h
Wall thickness	3 mm
Number of exposure/vacuum cycles	5

The response of the metals to the tritium pulses are shown in Figs. 150.51–150.53. In each figure (a) shows the calculated

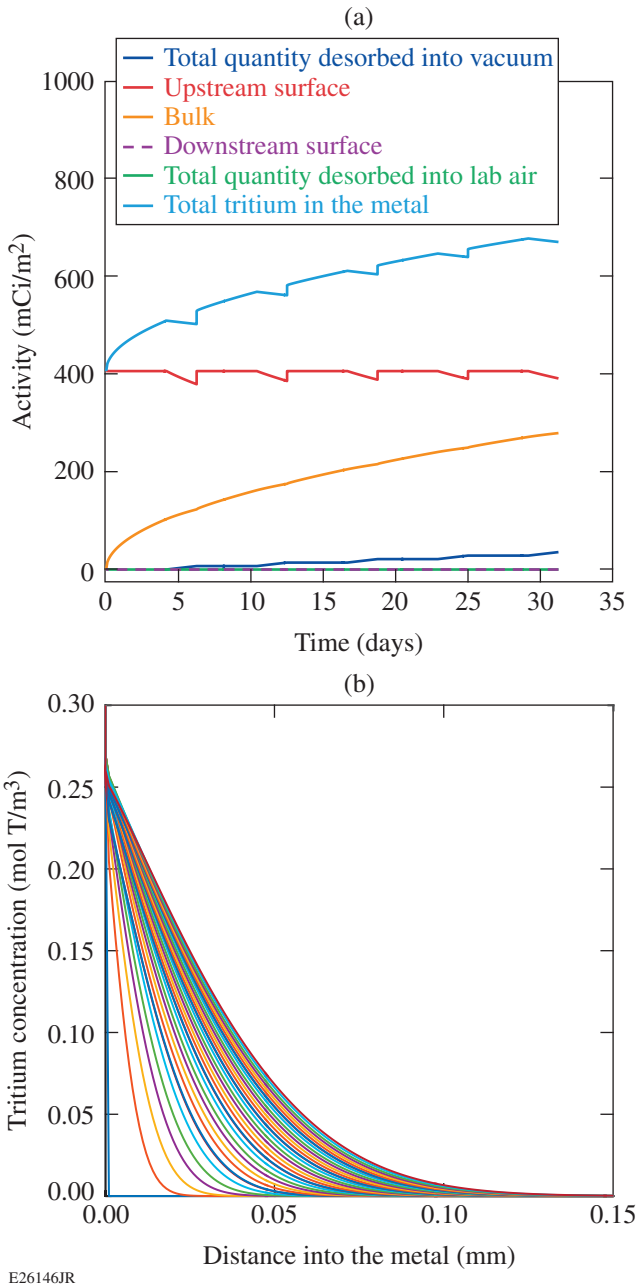

Figure 150.51
(a) Activity distribution and (b) tritium concentration profiles calculated for a stainless-steel wall exposed to repeated cycles of DT gas followed by vacuum desorption.

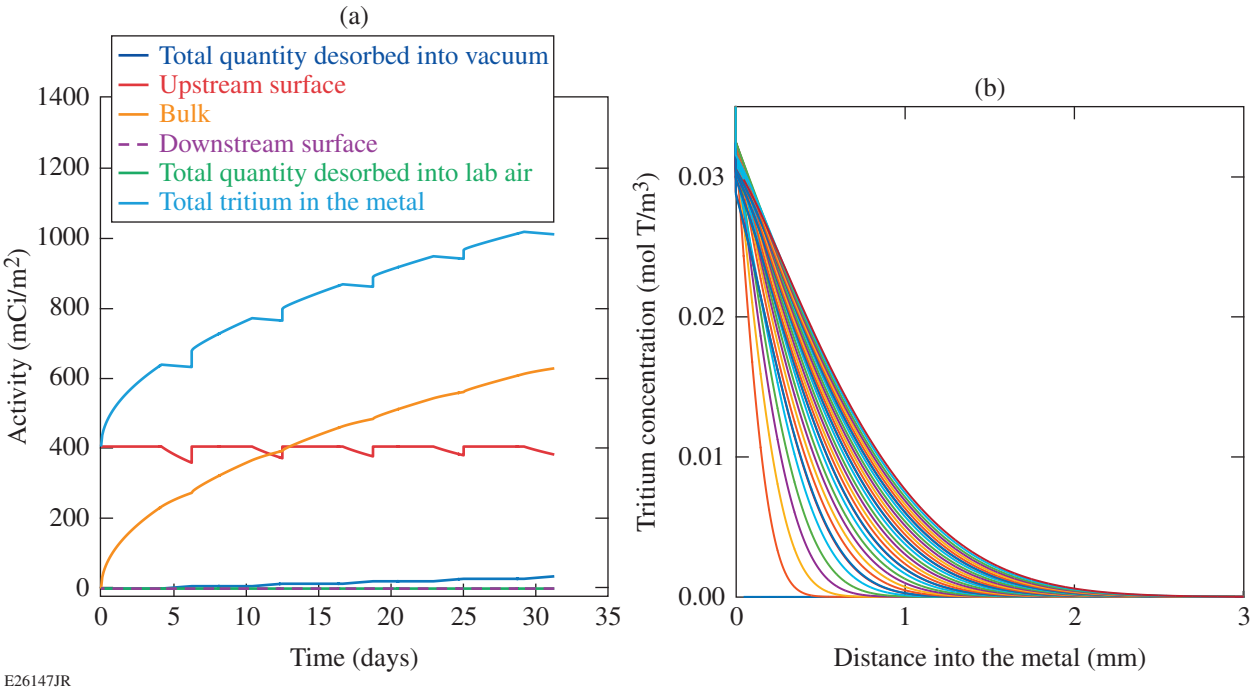

Figure 150.52
(a) Activity distribution and (b) tritium concentration profiles calculated for a copper wall exposed to repeated cycles of DT gas, followed by vacuum desorption.

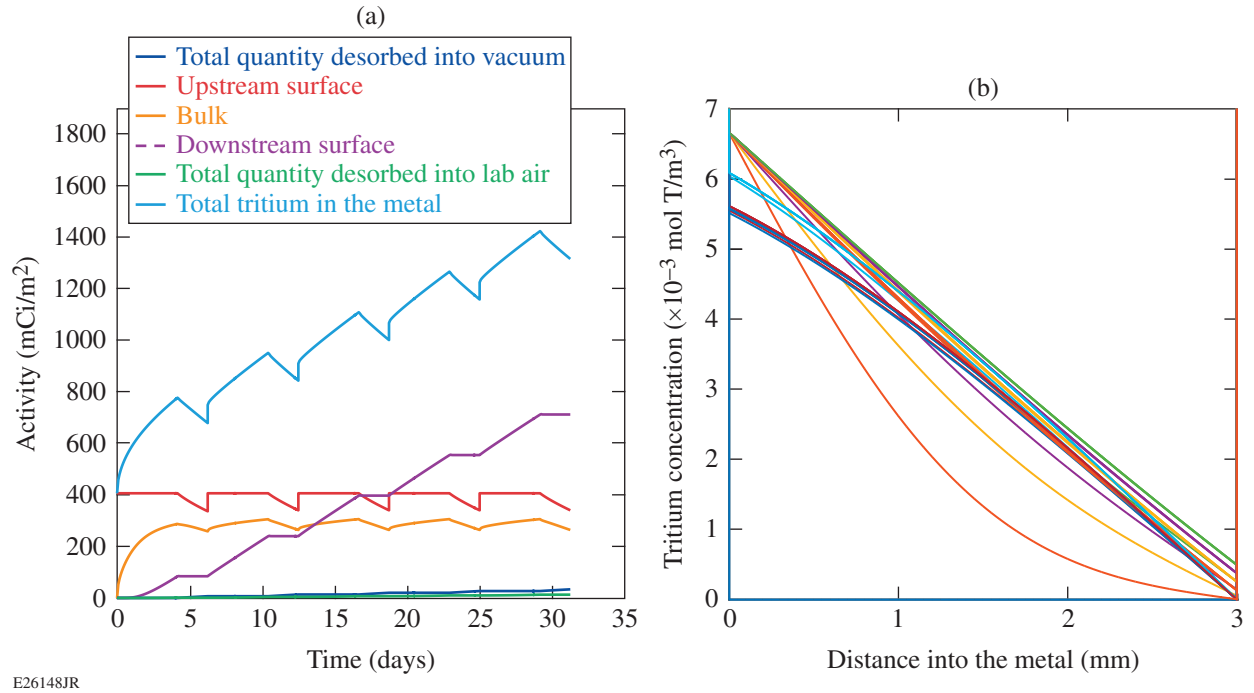

Figure 150.53
(a) Activity distribution and (b) tritium concentration profiles calculated for an aluminum wall exposed to repeated cycles of DT gas, followed by vacuum desorption.

quantities for tritium present on the upstream and downstream surfaces, tritium within the metal lattice, and the amount of tritium lost to the downstream side. The total tritium inventory present on the surfaces and in the lattice is plotted as well. In each figure (b) shows the evolution of the tritium concentration profiles in the metal lattice over the course of five exposure and vacuum cycles. In general, the activity distributions show that each wall absorbs tritium during each DT exposure. Additionally, while tritium desorbs from the inner wall when under vacuum, the duration of the exposure to vacuum is not long enough to allow a significant release of the absorbed tritium. Ultimately, this leads to the metal wall absorbing increasingly more tritium with each exposure-vacuum cycle. The tritium concentration profiles within the metal lattice show increasing penetration into the metal with each successive cycle. The exception is for aluminum, which attains steady-state permeation through the wall within the first exposure cycle.

The simulations show several notable differences among the three metals. The first difference is evident in the calculated concentration profiles within each metal. The profiles indicate that tritium permeates through aluminum much faster than the other two metals, such that steady-state permeation is achieved within the first DT exposure. Additionally, while the subsequent vacuum portions of each cycle serve to decrease the concentrations throughout the aluminum wall, steady-state permeation is reclaimed during the following DT exposure. For copper, a negligible quantity of tritium permeates through the wall and steady-state permeation is not achieved during the five cycles. Finally, permeation through stainless steel is the slowest, with no tritium reaching the downstream surface. This trend in tritium permeation rates follows the same trend in the tritium diffusivity through each metal: tritium diffusivity is slowest in stainless steel and quickest in aluminum. As a consequence, the calculated quantity of tritium desorbing from the downstream side of the wall is largest for aluminum and smallest for stainless steel.

Conclusions

QTRIMM, outlined in this article, allows one to calculate the tritium concentration profiles within a metal sample. This model represents a novel approach to assessing the migration of tritium into, out of, and within a metal. It accounts for high concentrations of tritium on metal surfaces. The model predicts the evolution of the tritium concentration profiles that develop during an exposure to tritium gas, during subsequent storage periods, and during iterative decontamination cycles. This article illustrates the application of QTRIMM to show the tritium concentrations within stainless steel that was exposed to tritium gas and then stored for 50 days. Additionally, QTRIMM was used to predict the changes in surface activity as a result of decontamination cycles. The model demonstrates two well-known phenomena: (1) tritium can "reappear" on a decontaminated surface and (2) the longer one waits to clean a contaminated surface, the harder it is to decontaminate the metal. Finally, QTRIMM was used to predict the quantities of tritium that can permeate through aluminum, copper, and stainless steel. The calculations show that the greatest quantity of tritium permeated through aluminum compared to copper or stainless steel of the similar thicknesses. As a result of the quicker diffusion of tritium through aluminum, the model predicts that aluminum will contain the largest quantity of tritium after several exposures to DT gas compared to the other two metals but it is expected to be decontaminated more quickly than the other two metals.

ACKNOWLEDGMENT

This material is based upon work supported by the Department of Energy National Nuclear Security Administration under Award Number DE-NA0001944, the University of Rochester, and the New York State Energy Research and Development Authority.

REFERENCES

1. N. Nakashio *et al*., Fusion Sci. Technol. **39**, 189 (2001).
2. K. Akaishi *et al*., J. Vac. Sci. Technol. A **26**, 321 (2008).
3. S. Naoe *et al*., Fusion Sci. Technol. **54**, 515 (2008).
4. R.-D. Penzhorn *et al*., Fusion Sci. Technol. **57**, 185 (2010).
5. T. Hirabayashi, M. Saeki, and E. Tachikawa, J. Nucl. Mater. **126**, 38 (1984).
6. M. Nishikawa *et al*., J. Nucl. Mater. **277**, 99 (2000).
7. R.-D. Penzhorn *et al*., J. Nucl. Mater. **353**, 66 (2006).
8. Y. Torikai and R.-D. Penzhorn, Fusion Sci. Technol. **67**, 615 (2015).
9. G. Münchow *et al*., Langmuir **24**, 8547 (2008).
10. R. A. Surette and R. G. C. McElroy, Fusion Technol. **14**, 1141 (1988).
11. M. Sharpe, W. T. Shmayda, and W. U. Schröder, Fusion Sci. Technol. **70**, 97 (2016).
12. W. T. Shmayda, M. Sharpe, A. M. Boyce, R. Shea, B. Petroski, and W. U. Schröder, Fusion Sci. Technol. **68**, 766 (2015).